Journal of Stress Analysis
Vol. 4, No. 1, Spring – Summer 2019
Bu-Ali Sina University

Ductile Failure Prediction of Friction Stir Welded AA7075-T6 Aluminum Alloy Weakened by a V-notch

A. Nouri*, M. Kazemi Nasrabadi
Aerospace Engineering Deparement, Shahid Sattari Aeronautical University of Science and Technology, Tehran, Iran.

Article info

Article history:
Received 23 July 2019
Received in revised form
10 September 2019
Accepted 15 September 2019

Keywords:
Friction Stir Welding (FSW)
Equivalent Material Concept (EMC)
Fracture toughness
Elastic-plastic behavior
Maximum Tangential Stress (MTS)
Mean Stress (MS)

Abstract

With increasing applications of the Friction Stir Welding (FSW), a proper study of the fracture behavior is required. In this research, fracture behavior of AA7075-T6 alloy joint made by FSW is investigated by evaluat-ing a fracture test on the Diagonally Loaded Square Plate (DLSP) specimen containing a V-notch, under various loading conditions. Significant plastic deformation takes place around the notch tip at the propagation instance, which shows the elastic-plastic behavior of the welded joint. Ductile failure needs some elastic-plastic fracture mechanics criteria, which are complex and time-consuming. To deal with this, the Equivalent Material Concept (EMC) was applied via replacing a virtual brittle material with a ductile material by equating the tensile behavior of the welded material. In order to predict the Load-Carrying Capacity (LCC) of the FSW DLSP specimens, the EMC was used, which is in conjunction with two brittle fracture criteria called the Maximum Tangential Stress (MTS) and the Mean Stress (MS). Finally, results indicate that with a slight difference, two mentioned criteria could predict the LLC of the V-notched specimens.

Nomenclature

2α	Notch length	d_c	Critical distance
E	Modulus of elasticity	K_{Ic}	Fracture toughness
$K_{Ic}^{V,\rho}$	Notch fracture toughness	$K_I^{V,\rho}$	Notch Stress Intensity Factor
L	Plate length	P	Applied force
r_c	Critical distance	λ_1	Eigenvalue
$\sigma_{\theta\theta}$	Tangential stress	β	Notch inclination angle
σ_c	Critical stress	σ_f^*	Ultimate strength
r_0	Distance between the Cartesian and the curvilinear coordinate systems	ρ	Notch radius

1. Introduction

Aluminum alloys are well-known materials due to their light weight and high specific strength, which are extensively used in modern industries. Recently, according to their preferable advantages the use of these alloys, especially AA7075 alloy, has increased in advanced aerospace structures. Typically, the alloy is joined by mechanical fastening, which leads to stress concentration and slow assembly. Moreover, conven-

*Corresponding author: A. Nouri (Assistant Professor)
E-mail address: anouri@ssau.ac.ir
http://dx.doi.org/10.22084/jrstan.2019.19695.1099
ISSN: 2588-2597

tional fusion welding methods have been neglected due to unbalanced grain distribution, degraded mechanical properties, and the existence of porosity in the weld region. In the past two decades, FSW has become a reliable method to join low weld ability 7XXX series Al alloys along with proper mechanical properties.

FSW is a solidstate joining process that was originally introduced by The Welding Institute [1]. The operation is conducted by rotation and transverse motion of a predesigned tool generating an exceptional quality joint with significantly lower residual stresses, [2]. Low cost, energy consumption, and environmental pollution in addition to desirable strength to weight ratio, turns FSW to one of the most appropriate alternative welding methods, especially in aerospace applications involving aluminum alloys [3]. Attractive features of this newly developed welding method led to a large number of studies, including micro and macro structural properties, mechanical properties, tool parameter effect, which have become the baseline of this study. Briefly, results of these published researches are summarized here. Understanding the effect of process parameters on the material flow behavior, microstructure formation, mechanical properties of friction stir welded joints, and finding the most effective parameters on properties of friction stir welds have been a major concern for researchers, [4], [5], and [6]. Considering the study of Rajakumar et al. [7], the predominant factors that have the most considerable influence on the fabricated joints are rotational speed, welding transverse speed, axial force, shoulder diameter, pin diameter, and tool material hardness; [7] it was also demon-strated that the well-defined parameter could provide high strength and void-free joint.

The various parameters affecting the weld quality during the FSW process involving the butt joining of AA7075 T6 were investigated by Bahemmat et al. [2]. Kumar et al. [8] studied the influence of the tool geometry on the FSW of an aluminum alloy with specific reference to microstructural development, defect formation, and mechanical response. Some researchers concentrated on hardness property of the welded joint. Moreira et al. [9] studied hardness of various regions of dissimilar friction stir welded of AA6061-T6 and AA6082-T6. The results showed that the maximum hardness occurs in the Nugget Zone (NZ) and the minimum occurs on the border between Thermo-Mechanically Affected Zone (TMAZ) and Heat Affected Zone (HAZ). Some scientists focused on the tensile strength of welded joints. For example in a study which was done by Palanivel et al. [10], various tool shapes and rotational speeds were used to achieve the highest tensile strength for dissimilar friction stir welded of AA5083 and AA6351 aluminum alloys. On the other hand, a study done by Mishra and Ma [11], illustrated that the tensile strength of friction stir welded joints of AA2024 aluminum alloy increases by enhancing the rotational and transverse speed. Furthermore, Cavaliere et al. [12] investigated the mechanical and microstructural properties of dissimilar friction stir welded of AA7075 and AA2024 aluminum alloys.

Considering the high potential of friction stir welding and the growth of its application, studying its fracture behavior is vital. Von-Strombeck et al. [13] studied the fracture toughness of different aluminum alloys, which had undergone the FSW process, by employing Compact Tension (CT) tests. Based on their observations, it was determined that the fracture toughness of the welded joints increases compared to the parent material. Dawes et al. [14] presented results about the fracture toughness of cracked specimens using three-point bending tests. According to the values obtained by Crack Tip Opening Displacement (CTOD) and J integral, the Nugget Zone (NZ) demonstrated higher fracture toughness than the base material. In another study on the friction stir welded lap joints of AA2024 and AA6063 aluminum alloys done by Kulekci et al. [15], the fracture toughness of welded joints was calculated. The results illustrated that the fracture toughness of FSW joints increases exponentially as the hardness reduces. The effect of sheet thicknesses of friction stir spot welding on lapshear specimens of Al 6061-T6 alloy was experimentally analyzed by Shahani and Farrhi [16].

In line with enormous industrial application of the aluminum alloys, there is always a possibility of failure due to fatigue. Cavaliere and Panella [17] studied the fatigue properties and the fatigue crack growth behavior of dissimilar friction stir welded joints of AA2024 and AA7075 aluminum alloys, produced with altering the position of the tool. Golestaneh and Ali [18] and also Golestaneh and Voon [19] investigated fatigue behavior of friction stir welded of AA2024-T6 sheets. Alavi and Shirazi, determined the thermal histories in copper sheets during a Friction Stir Welding butt joining process using the experimental and numerical models [20]. The fatigue life was predicted using linear elastic fracture mechanics based on the Paris model. Moreira et al. [21] studied the fatigue behavior of notched specimens of friction stir welded aluminum alloy AA6063-T6 sheets. Compared to the base material, welded specimens represented longer fatigue lives with generally the same order of magnitude.

Accordingly, few researches have been published to determine the fracture behavior of mode I, mode II, and I/II mixed mode loading conditions of joints made by the FSW technique. By using Crack Opening Displacement (COD) criterion, Sutton et al. [22] studied mode I fracture, which was performed on both base material and friction stir welded AA2024-T3 aluminum plate. Results from mode I fracture tests indicated that FSW joints have a through-thickness variation in fracture resistance.

In addition, Sutton et al. [23] and [24] investigated mixed I/II fracture of AA2024-T3 and AA2524-T351 friction stir weld. The COD values also demonstrated that transition from mode I to mode II dominant crack

growth occurs at lower loading angles for FSW. Recently, Torabi et al. [25] analyzed fracture of dissimilar Al-Al friction stir welded joints under tensile/shear loading; They employed cracked Semi-Circular Bending (SCB) specimens in order to predict the load carrying capacity of welded joints using Equivalent Material Concept (EMC) in conjunction with brittle fracture criteria. Comparison of the experimental results and theoretical predictions indicated that developed EMC criterion could accurately predict the load carrying capacity of the cracked specimens. In another study, Aliha et al. [26] investigated the mixed mode I/II fracture of Al-Cu friction stir welded joints. This study represented that the EMC criterion, in conjunction with brittle fracture criteria, can accurately predict the load carrying capacity of the welded joints.

In this investigation, first, AA7075-T6 aluminum plates were welded by the FSW, and then by evaluating a fracture test on the Diagonally Loaded Square Plate (DLSP) specimen containing a V-notch, under various loading conditions, fracture toughness was determined. The proposed specimen can produce full combinations of mode I and mode II loadings in the FSWed joint and also pure mode II loading condition. Eventually, the load carrying capacity data obtained from the experiments were compared to the theoretical values.

2. Experimental Works

2.1. Material

In this research, AA7075-T6 aluminum alloy was used due to its wide application in industry, especially in the aerospace. Considering the DLSP specimen dimensions and costs, the sheets were cut with dimensions of 210mm long, 70mm wide. The chemical compositions and mechanical properties of the used AA7075-T6 aluminum alloy are presented in Tables 1 and 2, respectively.

2.2. Welding Procedure

At first, all plates were machined to raise the accuracy and achieve fine butt welded joints. Choosing the perfect welding tool is one of the essential factors of FSW. In this study, a non-consumable tool made of H13 steel with the participation of 5% chromium, was used. Table 3 shows the chemical compositions extracted from ASTM-A681, Cormier et al. [27]. The shoulder and pin diameters were 18 and 5mm, respectively. The cylindrical pin used was 2.2mm in height, and the tool tilt angle was set at 3° to the normal direction of the plate. Two plates were butted together to avoid separation and keep specimens positions under applied forces caused by the tool during the process under control. The clamp was designed in such a way to keep the plates together, providing the sufficient force to carry out the friction stir welding as well as making the plate changing process faster. In this study, a vertical CNC machine, as a supplier of vertical and rotational speeds, was employed for friction stir welding. The plates positioning and the used milling machine are shown in Fig. 1. The selected process parameters were obtained after carrying out welding with various rotational and transverse speeds. However, in order to reduce cost and time and also not to need perfect weld in this study, first desirable obtained parameters which were intuitively flawless and defect free were chosen. The selected process parameters are 800 rpm and 20mm/min for rotational and transverse speeds, respectively. The appearance of a sample Al-Al joint can be seen in Fig. [2]. No surface defect in the weld zone was detected, which indicates the sound quality of the FSWed Al-Al joints.

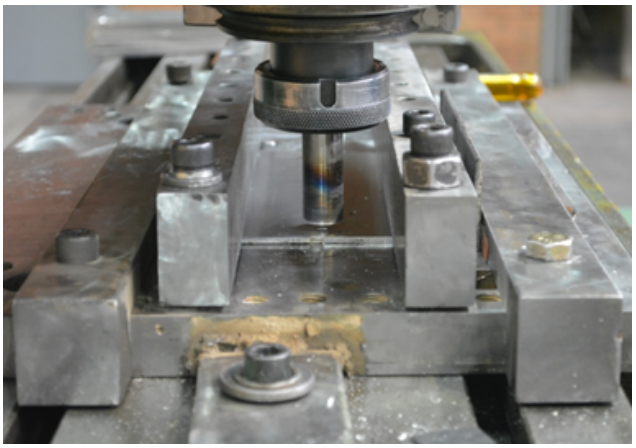

Fig. 1. Plate positioning and the FSW process.

Table 1
Chemical composition of used Al 7076-T6 [2].

Element	Si	Fe	Cu	Mn	Mg	Zn	Ni	Cr	Pb	Sn	Ti
Weight (%)	0.06	0.32	1.72	0.03	2.44	4.63	0.004	0.2	0.002	0.001	0.037
Element	B	Cd	Bi	Ca	P	Sb	V	Zr	Co	Li	Al
Weight (%)	0.001	0.001	0	0.001	0.001	0.001	0.007	0.017	0.003	0.001	90.5

Table 2
Tensile properties of Al 7075-T6 [2].

Material	Yield strength (MPa)	Ultimate strength (MPa)	Total elongation (%)	Elastic modulus (GPa)
Al 7075-T6	521	583	8	74

Table 3
Chemical compositions of used tool made of H13 steel [27].

Element	C	Cr	Mo	Si	V	Mn
Weight (%)	0.35	4.8	1.13	0.96	0.95	0.4

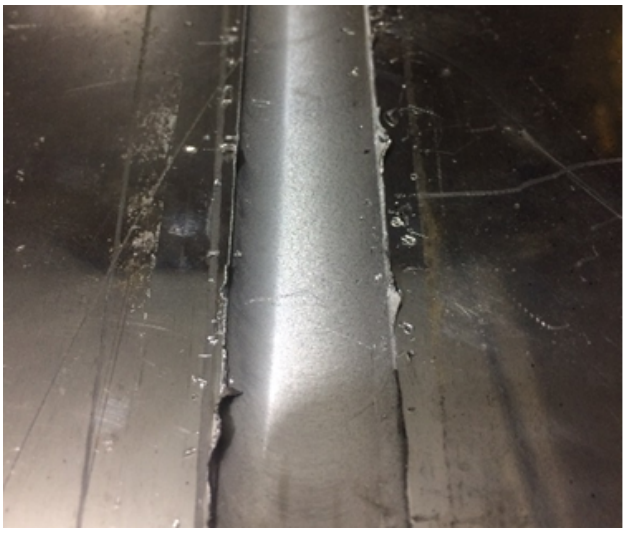

Fig. 2. Appearance of a sample friction stir welded Al-Al joint.

2.3. Specimen Preparation

The Diagonally Loaded Square Plate (DLSP) specimens containing a V-notch, under various loading condi-tions, were used in this study. The previous results, done by Ayatollahi and Aliha [28], illustrated that the DLSP specimen can provide pure mode I, pure mode II, and any mixed mode loading conditions in between. Fig. 3 schematically illustrates the DLSP specimen. The cited parameters 2α, β, ρ, $2a$, L, and P denote the notch angle, notch inclination angle, notch radius, twice the notch length, a square plate edge length, and applied force in the DLSP specimen, respectively. The values of $2a$, L, and 2α are listed in Table 4.

Table 4
Dimensions of the used DLSP specimen.

Length (L)	70mm
Twice the notch length ($2a$)	21mm
Notch angle (2α)	30degree

To cover different mode combinations, it is required to choose some different angles for β. Using finite element software, the desirable angles were calculated, which are equal to 0, 30, and 45 degrees for pure mode I, mixed mode I/ II, and pure mode II, respectively. Fig. 4 displays some manufactured DLSP specimens with explained β angle and thickness of 2.54mm, which were cut.

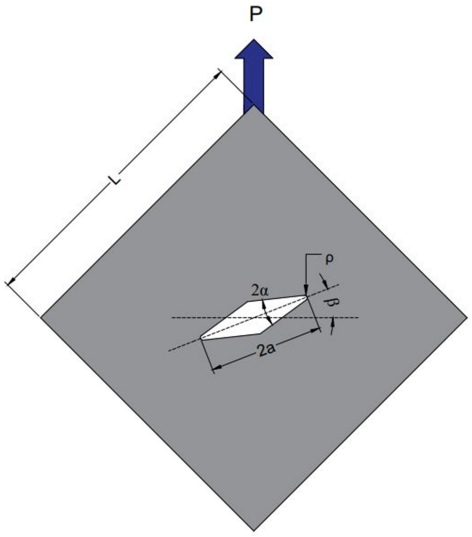

Fig. 3. Schematic of CSCB specimen.

2.4. Test Procedure

The produced DLSP specimens fracture tests were carried out under displacement-control conditions with a speed of 1mm/min, providing monotonic loading conditions. When the notch is horizontal (i.e., $\beta = 0$), the DLSP specimen is subjected to pure mode I loading. As the notch rotates, mixed mode I/II loading condition is provided, and $\beta = 45$ provides pure mode II loading.

The test was carried out three times for each notch angle, and the load-displacement curves and the critical loads (i.e., LCCs) were recorded. Figs. 5 and 6 represent the DLSP test set-up for Al7075-T6 friction stir welded butt joint and a sample attained load-displacement curve.

Additionally, Table 5 represents the experimentally extracted load carrying capacities of the DLSP specimens produced from the Al-Al friction stir welded joints. The image of specimen after fracture for three different angles are shown in Fig. 7.

Table 5
Report of the LCCs obtained experimentally for the DLSP specimens.

β	ρ	Load carrying capacity (N)		
		Test 1	Test 2	Test 3
0	1	12099	12123	12249
	2	12735	12992	13292
	4	15483	15001	14546
30	1	15814	13963	12101
	2	16348	15249	14159
	4	18184	18160	18173
45	1	18124	18120	18104
	2	19963	20049	20125
	4	12099	22505	22495

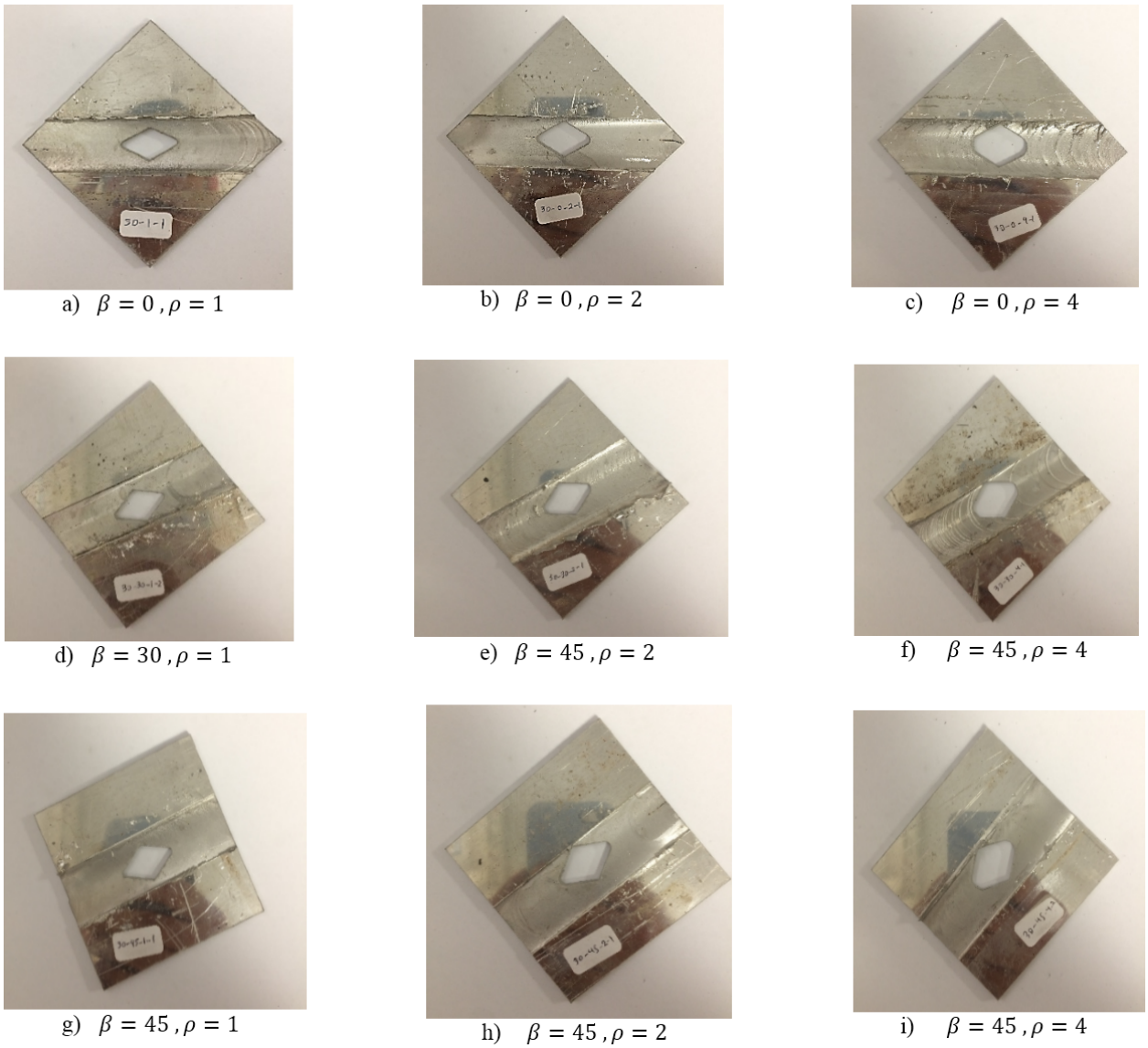

Fig. 4. The DLSP specimens with various notch angles designed for fracture study of welded Al-Al joints.

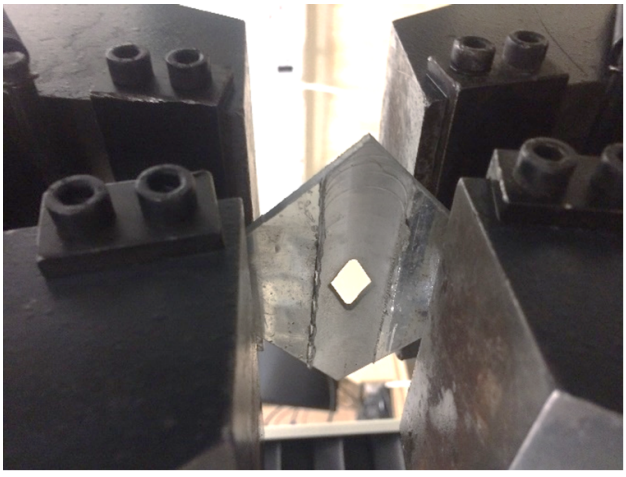

Fig. 5. A sample used test setup for the DLSP specimen Al-Al welded using FSW process under pure mode I.

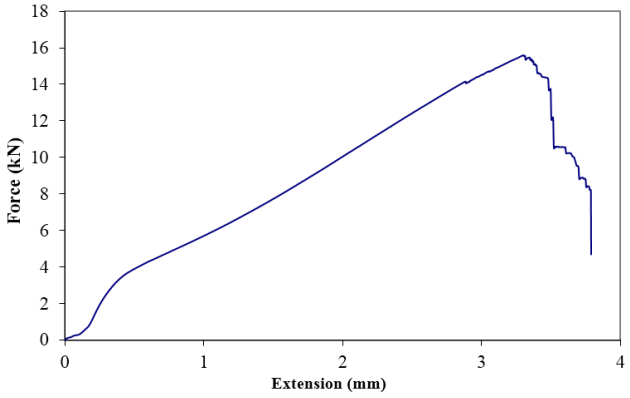

Fig. 6. Typical load-displacement curve obtained for $\beta = 0$ and $\rho = 4$ DLSP specimen.

Considerable roundness occurs at the notch tip after crack initiation, which is obvious with the naked eyes.

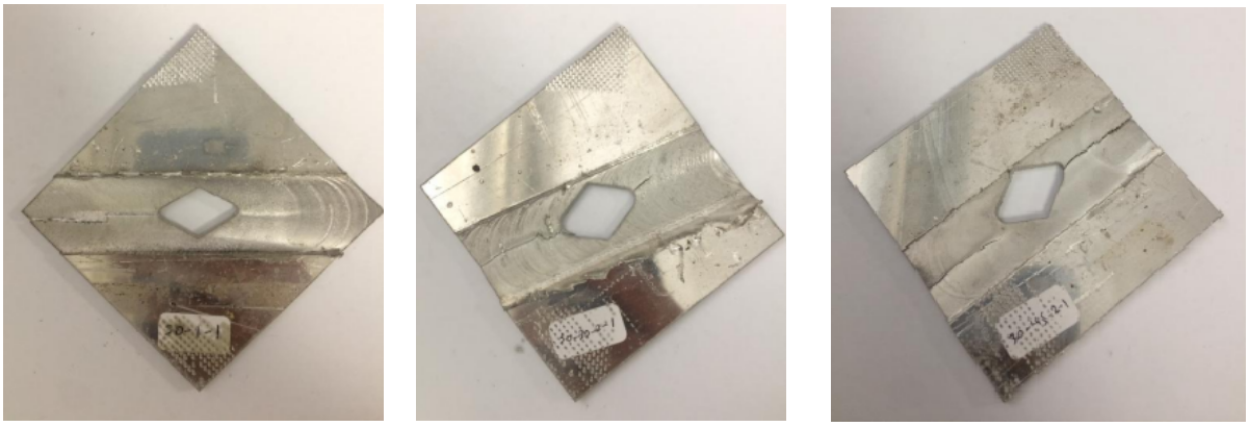

Fig. 7. The specimen after fracture for three different angle.

Regarding experimental observations, notable plastic deformation indicates that the welding zone behavior with remarkable precision is ductile. Moreover, to ensure the ductility of the material, obtained load-displacement curves of the tested DLSP specimens were checked. Existence of the significant nonlinear zones, until load-displacement curves reach the maximum load, proves the ductility of the welded joints. FSWed joint ductility yields the result that ductile failure criteria should be used to predict the load carrying capacity of the V-notched DLSP specimens. Since, elastic-plastic criteria are complicated and time-consuming, according to Torabi et al. [29], in this research, a newly developed criterion called the Equivalent Material Concept (EMC) was used to achieve critical loads.

In the next section, the EMC is briefly described, and how this concept can predict the load carrying capacities in conjunction with brittle fracture described is explained.

3. The Equivalent Material Concept

In this paper, in order to study the fracture behavior of ductile materials, a new method, introduced by Torabi [30], called the Equivalent Material Concept (EMC) is used. One of the features of this concept is that there is no need for complicated and time-consuming elastic-plastic analysis. According to the EMC, a ductile material is equivalent to a virtual brittle material. In such a way, absorbed strain energy density up to the peak point is equal to this value for a virtual brittle material with the same modulus of elasticity and fracture toughness.

Based on the EMC, a ductile material is transformed into a brittle material with the same elastic modulus, but with an unknown ultimate strength (σ_f^*) which is calculated by equating the SED of a ductile material with the SED of a virtual brittle material. A sample tensile stress-strain curve for a ductile material is shown in Fig. 8. Additionally, Fig. 9 presents a brittle material stress-strain, which the SED to the fracture is highlighted schematically. In order to calculate the SED for the ductile materials associated with the crack initiation, the gray area should be computed. This area can be easily calculated using simple mathematical software.

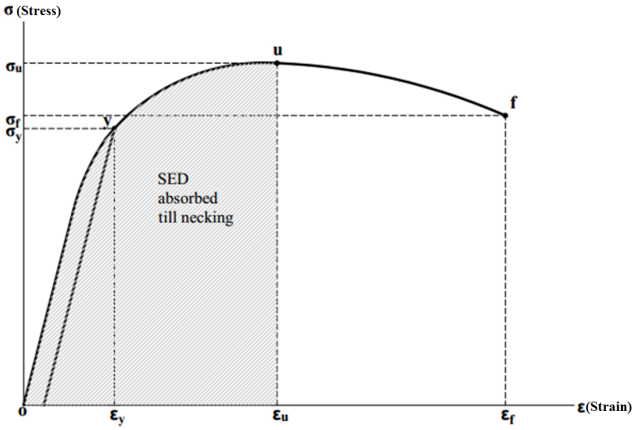

Fig. 8. Typical tensile stress-strain curve for a ductile material.

The specified gray area is equal to $\sigma_f^*/2E$. According to EMC, the gray areas in Figs. 8 and 9 should be equal. Therefore:

$$(SED)_{EMC} = \frac{\sigma_f^{*^2}}{2E} \rightarrow \sigma_f^* = \sqrt{2E(SED)_{EMC}} \quad (1)$$

The obtained tensile strength of the equivalent material (σ_f^*) is a key to use brittle fracture criteria for ductile failure predictions.

Calculating the virtual tensile strength σ_f^*, leads into using brittle fracture criteria to predict LLCS of FSWed DLSP specimens. In the next section, two used brittle fracture criteria, namely the Maximum Tangential Stress (MTS) and Mean Stress (MS) are presented.

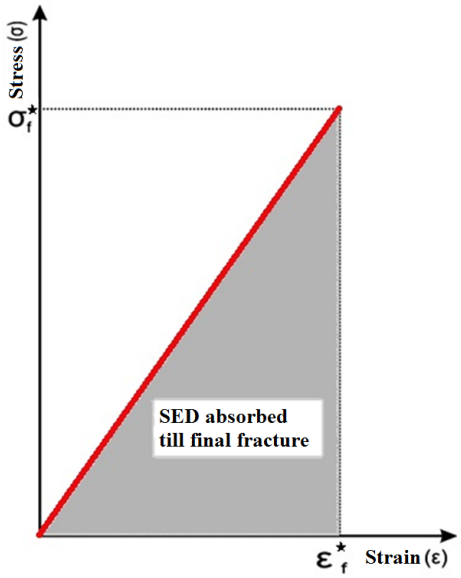

Fig. 9. SED absorbed by the equivalent material until the final fracture.

4. Brittle Fracture Criteria

As previously mentioned, for estimation of the fracture load, at first, with the introduction of the EMC and equating a ductile material with a virtual brittle material, term of use for brittle fracture criteria is provided. In this study, for the brittle fracture, two of the validated criteria namely, the classical Maximum Tangential Stress (MTS) and Mean Stress (MS) criteria were used to predict the load carrying capacity of the friction stir welded Al-Al butt joints. Herein, a short description of two named brittle criteria is presented.

4.1. Maximum Tangential Stress (MTS) Criterion

The Maximum Tangential Stress (MTS) criterion is an accepted criterion in analyzing the brittle fracture for specimens containing crack and various notch shapes. Erdogan and Sih [31] originally introduced this method for mixed mode I/II fracture prediction in brittle specimens weakened by sharp cracks. Based on the V-notched Maximum Tangential Stress (VMTS) criterion, brittle fracture occurs as the tangential stress $\sigma_{\theta\theta}$ reaches the material critical stress σ_c at a specified critical distance r_c ahead of the notch tip. It should be noted that both the critical stress σ_c and the critical distance r_c are autonomous from loading and geometric condition and they are related to the material properties, Aliha and Ayatollahi [32]. Fig. 10 shows the MTS criterion for V-notched components and also critical distances schematically.

As it is shown in Fig. 10, the distance between the maximum tangential stress and the origin of the coordinate system is called the critical distance (r_c). At first, to predict the load carrying capacity of the brittle materials using VMTS, the critical distance r_c and the critical stress σ_c, which are the material properties, should be calculated. The calculation process of the critical stress σ_c was explained in the EMC section, and r_c can be computed by the following equation:

$$r_c = \frac{1}{2\pi}\left(\frac{K_{Ic}}{\sigma_c}\right)^2 \tag{2}$$

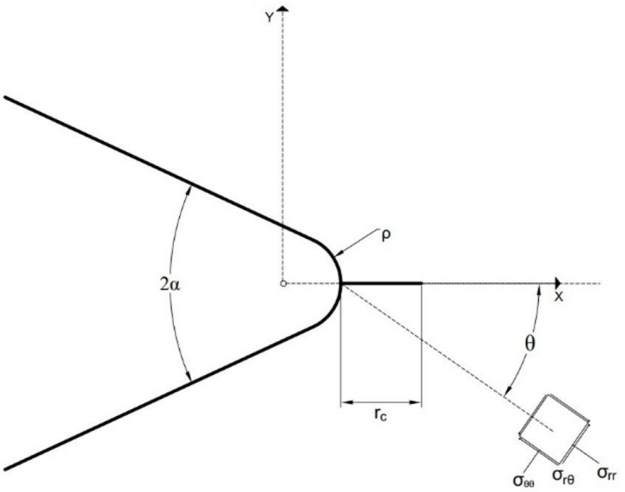

Fig. 10. A schematic view of the VMTS criterion.

The needed values of this equation are the calculated critical stress σ_c and the fracture toughness of the material K_{Ic}.

The load carrying capacity of the V-notched specimens can be predicted by means of the VMTS criterion in conjunction with the EMC. In this study, this combined criterion is named EMC-VMTS criterion. A Finite Element (FE) model of the DLSP specimens should be simulated, and a random unit load should be applied to the component. Afterward, at first, the tangential stresses on the notch tip should be recognized and the maximum tangential stress on this edge should be determined. A hypothetical line is considered between the specified point and the coordinate center and the critical distance r_c which is along this line should be computed. The tangential stress is determined at the calculated critical distance r_c. Since there is a linear relationship between the load and the tangential stress, the applied load is increased while the obtained tangential stress at the critical distance r_c is equal to the calculated critical stress σ_c. Such a load is a theoretical estimation of the LLC of the V-notched specimen.

4.2. Mean Stress (MS) Criterion

Mean Stress (MS) criterion has the same attitude as MTS criterion, but the difference is that the average of tangential stress over a specified critical distance ahead of the notch tip is calculated as the critical stress of

the fracture. As a result of the MS criterion, when the average value of the tangential stresses $\sigma_{\theta\theta}$ from the notch tip to the critical distance d_c, is equal to critical stress σ_c, brittle fracture takes place.

The named critical distance in the MS criteria d_c is calculated by the following equation, provided by Seweryn et al. [33]:

$$d_c = \frac{2}{\pi}\left(\frac{K_{Ic}}{\sigma_c}\right)^2 \tag{3}$$

Same as the explained EMC-VMTS criterion, the LCC of DLSP specimens containing a V-notch can be predicted using the EMC-VMS criterion. Again, a schematic view of the VMS criterion is shown in Fig. 11. To predict the load-carrying capacity, the same procedure described in subsection 4.1 can be used, except that a line should be considered from the notch tip to the specific point known a critical d_c, which is demonstrated in Fig. 11, then, an average of tangential stress over this line should be calculated. Like the EMC-MTS, the applied load should be expanded until the calculated mean stress reaches the virtual obtained critical stress σ_c. This obtained load is the predicted LCC by means of the EMC-VMS criterion.

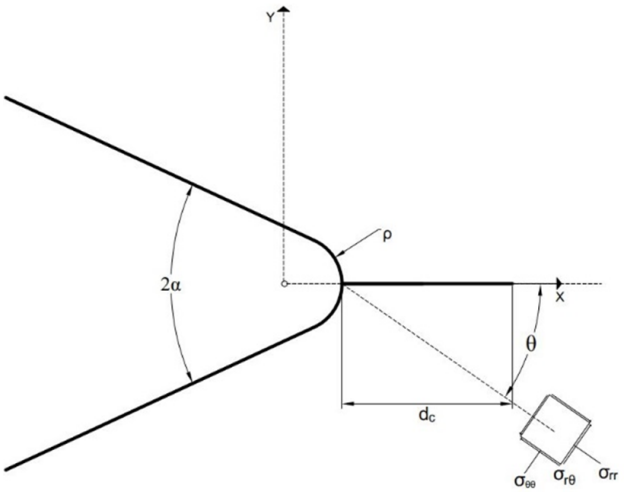

Fig. 11. A schematic view of the VMS criterion.

4.3. Evaluation of the Critical Loads

As previously mentioned, both the EMC-VMTS and the EMC-VMS criteria are employed to predict the load carrying capacity of the friction stir welded (DLSP) specimens. For this purpose, the values of critical distances and critical stress are required. Based on the EMC, ductile material equals to a virtual brittle material with the same elastic modulus with the unknown tensile strength σ_f^*. With the substitution of the calculated tensile strength as a critical stress σ_c, the theatrical load can be predicted without performing time-consuming and complicated elastic-plastic analyses. The expressions of the critical distances r_c and d_c for EMC-VMTS and EMC-VMS criteria, respectively are as following equations:

$$r_c = \frac{1}{2\pi}\left(\frac{K_{Ic}}{\sigma_f^*}\right)^2 \tag{4}$$

$$d_c = \frac{2}{\pi}\left(\frac{K_{Ic}}{\sigma_f^*}\right)^2 \tag{5}$$

5. Results and Discussion

The prerequisites for theoretically obtaining the LLCs by means of two introduced criteria EMC-MTS and EMC-MS were expressed in the previous sections. In this section, the predicted loads are calculated and compared with the obtained result of the experimental test.

5.1. Mechanical Properties of the FSW Zone

Before any process, for upcoming calculation, it is necessary to extract mechanical properties and material behavior of Al-Al joints made of FSW. As it was explained in the EMC section, a ductile material is considered as a brittle material and by use of macro structural properties of a material, which means stress-strain curve combined is with brittle fracture criteria, the load carrying capacities of the V-notched DLSP specimens can be predicted. Based on the EMC, it is assumed that the absorbed strain energy density of a ductile material is equal to this value for a virtual brittle material with the same elastic modulus. Thus, it is needed to extract the tensile stress-strain curve of a friction stir welded components. The dog-bone specimen for tension test is illustrated in Fig. 12.

The dog-bone specimen of AA7075-T6

The dog-bone specimen of welded AA7075-T6

Fig. 12. The dog-bone specimens.

The Fig. 13 shows the engineering and true stress-strain curves of the welded AA7075-T6 obtained from proper dog-bone specimen. The SED of a ductile material is calculated up to the ultimate strength of the material, so the engineering curve is used to find the ultimate point and the true curve is needed for SED calculation. Furthermore, the required tensile properties are obtained and presented in Table 6.

Table 6
Required tensile properties of the welded Al-Al joint.

Elastic modulus (GPa)	Yield strength (MPa)	Ultimate strength (MPa)	Elongation (%)
71	221	232	10

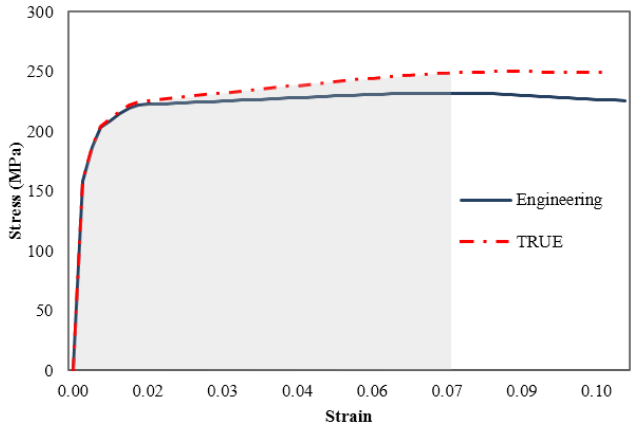

Fig. 13. Extracted stress-strain curves of the FSW joint and area under curved is hatched.

5.2. Calculation of the Equivalent Material Strength

To calculate the tensile strength of the equivalent material (σ_f^*) the needed stress-strain curves were obtained. Simple mathematical software was employed to calculate the area under the curve, which is shown in Fig. 13. The calculated value of the SED is equal to 2.08MPa. The tensile strength of the equivalent material can easily be obtained by substituting the calculated SED value equal to 2.08MPa and the elastic modulus of the Al-Al friction stir welded joint $E = 71$GPa into Eq. (1). Calculated σ_f^* is equal to 544MPa.

5.3. Fracture Toughness of the Friction Stir Welded Joint

According to Eqs. (4) and (5) to calculate critical distances r_c and d_c, the fracture toughness of material K_{Ic} is required. However, these equations need plane-strain fracture toughness K_{Ic}, which is a material property and is independent of the thickness and geometry of the component, the apparent fracture toughness (K_c) can also be used if components have a small thickness [34, 35]. In this study, the fracture toughness value was measured by means of the pure mode I fracture experiment results of the DLSP specimen. According to the MS and MTS criteria, fracture occurs under mode I condition when the value of mode I Notch Stress Intensity Factor (NSIF) $K_I^{V,\rho}$ reaches the notch fracture toughness $K_{Ic}^{V,\rho}$. Eq. (6) is used to calculate $K_I^{V,\rho}$ parameter.

$$K_I^{V,\rho} = \frac{\sqrt{2\pi}\sigma_{\theta\theta}(r_0, 0) r_0^{1-\lambda_1}}{1 + \omega_1} \tag{6}$$

In Eq. (6), $\sigma_{\theta\theta}(r_0, 0)$ is the tangential stress on the notch tip. λ_1 is an eigenvalue, r_0 is the distance between the Cartesian and the curvilinear coordinate systems which are shown in Figs. 10 and 11, and ω_1 is an auxiliary parameter which depends on the notch angle. r_0 and ω_1 which can be written as the following equations:

$$r_0 = \frac{q-1}{q}\rho, \qquad q = \frac{2\pi - 2\alpha}{\pi} \tag{7}$$

where ρ is the notch radius and 2α is the notch opening angle which is equal to $\frac{\pi}{6}$ in this study.

$$\omega_1 = \frac{q}{4(q-1)}\left[\frac{x_{d1}(1+\mu_1) + x_{c1}}{1 + \lambda_1 + x_{b1}(1-\lambda_1)}\right] \tag{8}$$

where the described parameters λ_1, μ_1, x_{b1}, x_{c1} and x_{d1} are presented in [36] for various notch opening angles.

This fracture toughness is achieved by considering the simulated mode I fracture of the welded DLSP specimen as a primary input. Therefore, mode I fracture of the component was simulated in ABAQUS, a finite element software, and the average load of experimental loads of mode I ($\beta = 0$) was considered as an input load. By substituting $\sigma_{\theta\theta}$, which was obtained directly from the simulated mode I fracture and also substituting calculated r_0 and ω_1 in the Eq. (6), K_c can be easily achieved and is equal to 30MPa$\sqrt{m}$. Fig. 14 demonstrates a sample mesh pattern for DLSP specimen subjected to pure mode I loading.

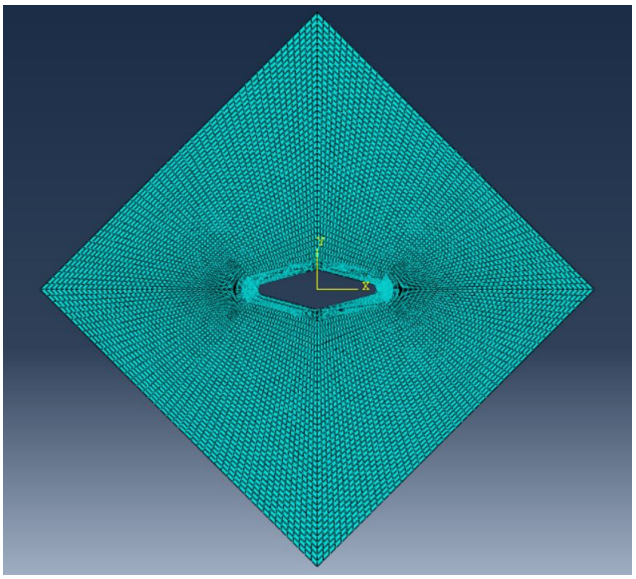

Fig. 14. A simulated model for DLSP specimen under pure mode I loading, Quad structured mesh is widely and sweep type is used around the notch tip.

5.4. Prediction of the Critical Load

In order to apply VMTS and VM criteria in conjunction with the equivalent material concept for the LLCs prediction, it is necessary to first, clarify linear elastic stress distribution. These stresses should be obtained at the critical distances for both EMC-VMTS and EMC-VMS criteria.

As previously mentioned, r_c and d_c as critical distances can be calculated by substituting K_c and σ_f^* which were given in the above calculations and are equal to $30\text{MPa}\sqrt{m}$ and 544MPa, respectively into Eqs. (4) and (5). This substitution leads r_c and d_c to be equal to 0.4 and 1.6mm for EMC-VMTS and EMC-VMS, respectively. For each V-notch angle, simulation was modeled in the ABAQUS FE software. For this purpose, DLSP specimens with the related dimensions are presented in Table 4.

Models subjected to the unit load and boundary conditions were performed. With respect to mesh independency, a uniform mesh was introduced to the model and the tangential stress distribution was generated. Due to the above calculated critical distances, the maximum tangential stress on the notch tip was considered and tangential stresses at the critical distance along the line which connects the coordinate center and the maximum tangential stress on the notch tip were read. Obtained tangential stresses were compared to the critical value of $\sigma_f^* \cong 544\text{MPa}$. Due to linearity between stresses and loads, the conducted loads were intensified, as obtained tangential stresses reach the critical value. This process leads to load carrying capacities of the V-notched DLSP specimens for EMC-VMTS criterion. Such procedure was done for the EMC-VMS criterion with a critical distance which is equal to 1.6mm to the notch tip.

In Figs. 15 to 17, the LLCs of DLSP specimens based on the EMC-VMTS and EMC-VMS criteria versus experiment results are compared for notch radius 1, 2 and 4mm, respectively. These figures confirm the validation of the Equivalent Material Concept in conjunction with VMTS and VMS criteria. According to the obtained results, it is evident that by increasing the contribution of the mode II loading than mode I, the discrepancy is heightened. The discrepancies of the theoretically predicted loads are presented in Table 7. This table shows that theoretical and experimental discrepancies are equal to 5.2% for EMC-VMTS criterion and 3.2% for EMC-VMS criterion, which means that both employed criteria can predict friction stir welded joints, which are containing V-notch, with fairly high accuracy. Although the EMC-VMS criterion can calculate the critical loads more precise than the EMC-VMTS criterion, due to simplicity and not a huge discrepancy, the EMC-VMTS is preferred in the viewpoint of engineering design.

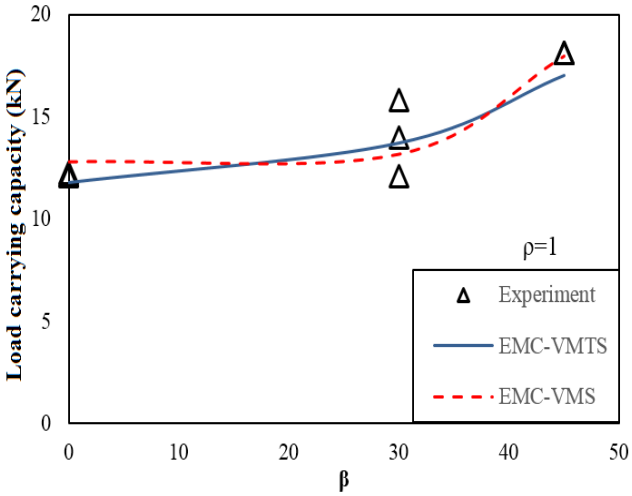

Fig. 15. Variations of LCC versus the notch inclination angle for $\rho = 1$.

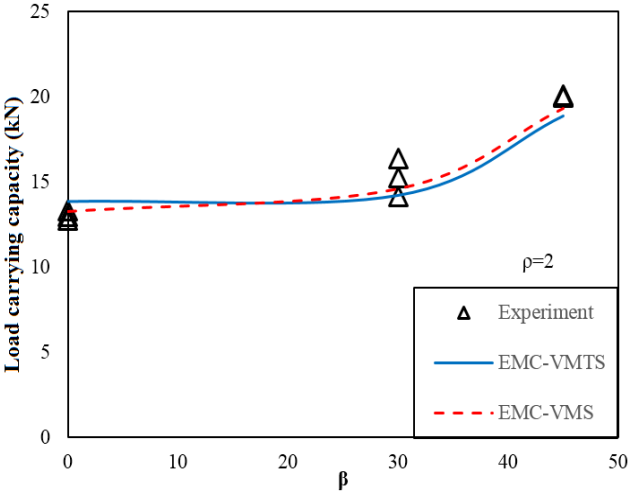

Fig. 16. Variations of LCC versus the notch inclination angle for $\rho = 2$.

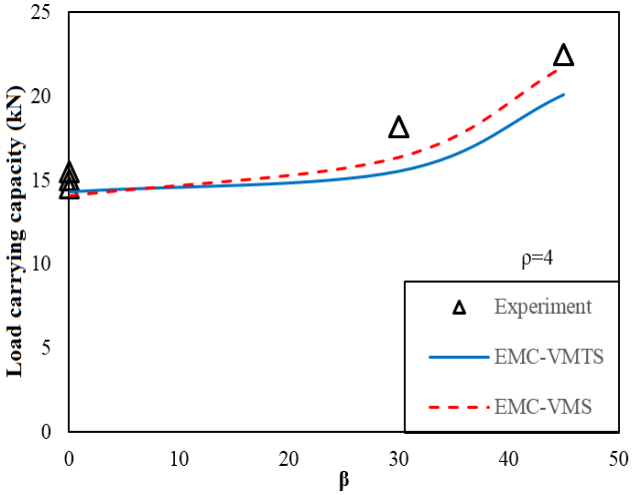

Fig. 17. Variations of LCC versus the notch inclination angle for $\rho = 4$.

Table 7
The discrepancy between theoretical and experimental results.

β (deg.)	0	30	45
Discrepancy of EMC-VMTS criterion (%)	0	7.6	8
Discrepancy of EMC-VMS criterion (%)	0	6.8	2.7
Mean discrepancy for EMC-VMTS criterion (%)		5.2	
Mean discrepancy for EMC-VMS criterion (%)		3.2	

6. Conclusions

As the FSW is a trending welding method in industry, several researches have been done in this field. In this study, the DLSP specimens were employed on the friction stir welded plates of AA7075-T6 aluminum alloy. The sound quality of the FSW was reached and load carrying capacities of the components were experimentally and theoretically investigated under mode I, mixed mode I/ II, and mode II loadings. Since the AA7075-T6 aluminum alloy is a ductile material which was confirmed in the context, the LLCs were predicted by means of the EMC, which is preferred to complex and time-consuming elastic-plastic analysis, in conjunction with two stress based VMTS and VMS brittle criteria. It was reported that both EMC-VMTS and EMC-VMS criteria could acceptably predict the LCCs and the difference between experimental loads and theoretical loads is low. Taking into design goals, each of these two explained criteria could be used for ductile failure predictions of friction stir welded joints.

References

[1] W.M. Thomas, E.D. Nicholas, J.C. Needham, M.G. Murch, P. Temple-Smith, C.J. Dawes, Friction stir butt welding, International Patent Application No. PCT/GB92/0220, (1991).

[2] P. Bahemmat , M.K. Besharati, M. Haghpanahi, A. Rahbari, R. Salekrostam, Mechanical, micro-, and macrostructural analysis of AA7075–T6 fabricated by friction stir butt welding with different rotational speeds and tool pin profiles, Proc. Inst. Mech. Eng. Part B: J. Eng. Manuf., 224(3) (2010) 419-433.

[3] W. Kim, B.C. Goo, S.T. Won, Optimal design of friction stir welding process to improve tensile force of the joint of A6005 extrusion, Mater. Manuf. Process., 25(7) (2010) 637-643.

[4] M. Peel, A. Steuwer, M. Preuss, P.J. Withers., Microstructure, mechanical properties and residual stresses as a function of welding speed in aluminium AA5083 friction stir welds, Acta Mater., 51(16) (2003) 4791-4801.

[5] C.M. Chen, R. Kovacevic, Finite element modeling of friction stir welding-thermal and thermo-mechanical analysis, Int. J. Tools Manuf., 43(13) (2003) 1319-1326.

[6] H. Schmidt, J. Hattel, J. Wert, An analytical model for the heat generation in friction stir welding, Model. Simul. Mater. Sci. Eng., 12 (2004) 143-157.

[7] S. Rajakumar, V. Balasubramanian, Establishing relationships between mechanical properties of aluminium alloys and optimised friction stir welding process parameters, Mater. Des., 40 (2012) 17-35.

[8] K. Kumar, S.V. Kailas, T.S. Srivatsan, Influence of tool geometry in friction stir welding, Mater. Manuf. Process., 23(2) (2008) 188-194.

[9] P.M.G.P. Moreira, T. Santos, S.M.O. Tavares, V. Richter-Trummer, P. Vilaça, P.M.S.T. de Castro, Mechanical and metallurgical characterization of friction stir welding joints of AA6061-T6 with AA6082-T6, Mater. Des., 30(1) (2009) 180-187.

[10] R. Palanivel, P.K. Mathews, N. Murugan, I. Dinaharan, Effect of tool rotational speed and pin profile on microstructure and tensile strength of dissimilar friction stir welded AA5083-H111 and AA6351-T6 aluminum alloys, Mater. Des., 40 (2012) 7-16.

[11] R.S. Mishra, Z.Y. Ma, Friction stir welding and processing, Mater. Sci. Eng. R: Reports., 50(1-2) (2005) 1-78.

[12] P. Cavaliere, R. Nobile, F.W. Panella, A. Squillace, Mechanical and microstructural behaviour of 2024-7075 aluminium alloy sheets joined by friction stir welding, Int. J. Mach. Tools Manuf., 46(6) (2006) 588-594.

[13] A. Von-Strombeck, J.F. Dos-Santos, F. Torster, P. Laureano, M. Kocak, Friction Toughness Behaviour of Friction Stir Welding Joints on Aluminum Alloys. First Int, Symp. Frict. Stir Welding, Thousand Oaks, California, USA, (1999).

[14] M.G. Dawes, S.A. Karger, T.L. Dickerson, J. Przydatek, Strength and fracture toughness of friction stir welds in aluminum alloys, Proc. 2nd Int. Frict. Stir Weld. Symp., (2000).

[15] M.K. Kulekci, I. Sevim, U. Esme, Fracture toughness of friction stir-welded lap joints of aluminum alloys, J. Mater. Eng. Perform., 21(7) (2012) 1260-1265.

[16] A.R. Shahani, A. Farrahi, Effect of sheet thickness on fatigue behavior of friction stir spot weld of Al 6061-T6 lap-shear configuration, J. Stress Anal., 3(1) (2018) 61-68.

[17] P. Cavaliere, F. Panella, Effect of tool position on the fatigue properties of dissimilar 2024-7075 sheets joined by friction stir welding, J. Mater. Process. Technol., 206(1-3) (2008) 249-255.

[18] A.F. Golestaneh, A. Ali, M. Zadeh, Modelling the fatigue crack growth in friction stir welded joint of 2024-T351 Al alloy, Mater. Des., 30(8) (2009) 2928-2937.

[19] A.F. Golestaneh, A. Ali, W.S. Voon, M.F. Mastapha, M.Z. Mohammadi, Simulation of fatigue crack growth in friction stir welded joints in 2024-T351 Al alloy, Suranaree J. Sci. Technol., 15(4) (2008) 271-285.

[20] A. Alavi Nia, A. Shirazi, A numerical and experimental investigation into the effect of welding parameters on thermal history in friction stir welded copper sheets, J. Stress Anal., 2(1) (2017) 1-9.

[21] P.M.G.P. Moreira, F.M.F. de Oliveira, P.M.S.T. de Castro, Fatigue behaviour of notched specimens of friction stir welded aluminium alloy 6063-T6, J. Mater. Process. Technol., 207(1-3) (2008) 283-292.

[22] M.A. Sutton, A.P. Reynolds, B. Yang, R. Taylor, Mixed mode I / II fracture of 2024-T3 friction stir welds, Eng. Fract. Mech., 70(15) (2003) 2215-2234.

[23] M.A. Sutton, A.P. Reynolds, B. Yang, R. Taylor, Mode I fracture and microstructure for 2024-T3 friction stir welds, Mater. Sci. Eng. A, 354(1-2) (2003) 6-16.

[24] M.A. Sutton, A.P. Reynolds, J. Yan, B. Yang, N. Yuan, Microstructure and mixed mode I / II fracture of AA2524-T351 base material and friction stir welds, Eng. Fract. Mech., 73(4) (2006) 391-407.

[25] A.R. Torabi, M.H. Kalantari, M.R.M. Aliha, Fracture analysis of dissimilar Al-Al friction stir welded joints under tensile/shear loading, Fatigue Fract. Eng. Mater. Struct., 41(9) (2018) 2040-2053.

[26] M.R.M. Aliha, M.H. Kalantari, S.M.N. Ghoreishi, A.R. Torabi, S. Etesam, Mixed mode I/II crack growth investigation for bi-metal FSW aluminum alloy AA7075-T6/pure copper joints, Theor. Appl. Fract. Mech., 103 (2019) 102243.

[27] D. Cormier, O. Harrysson, H. West, Characterization of H13 steel produced via electron beam melting, Rapid Prototyp J., 10(1) (2004) 35-41.

[28] M.R. Ayatollahi, M.R.M. Aliha, Analysis of a new specimen for mixed mode fracture tests on brittle materials, Eng. Fract. Mech., 76(11) (2009) 1563-153.

[29] A.R. Torabi, A. Campagnolo, F. Berto, Large-scale yielding failure prediction of notched ductile plates by means of the linear elastic notch, Fract. Mech. Strength Mater., 49(2) (2017) 224-433.

[30] A.R. Torabi, Estimation of tensile load-bearing capacity of ductile metallic materials weakened by a V-notch: The equivalent material concept, Mater. Sci. Eng. A, 536 (2012) 249-255.

[31] F. Erdogan, GC. Sih, On the crack extension in plates under plane loading and transverse shear, J. Basic Eng., 85 (1963) 519-525.

[32] M.R.M. Aliha, M.R. Ayatollahi, Analysis of fracture initiation angle in some cracked ceramics using the generalized maximum tangential stress criterion, Int. J. Solids Struct., 49(13) (2012) 1877-1883.

[33] A. Seweryn, S. Poskrobko, Z. Mróz, Brittle fracture in plane elements with sharp notches under mixed-mode loading, J. Eng. Mech., 123(6) (1997) 535-543.

[34] A.R. Torabi, M. Alaei, Application of the equivalent material concept to ductile failure prediction of blunt V-notches encountering moderate-scale yielding, Int. J. Damage Mech., 25(6) (2016) 853-877.

[35] A.R. Torabi, R. Habibi, Investigation of ductile rupture in U-notched Al 6061-T6 plates under mixed mode loading, Fatigue Fract. Eng. Mater. Struct., 39(5) (2016) 551-565.

[36] S. Filippi, P. Lazzarin, R. Tovo, Developments of some explicit formulas useful to describe elastic stress fields ahead of notches in plates, Int. J. Solids Struct., 39(17) (2002) 4543-4565.